JOURNAL OF THERMOPHYSICS AND HEAT TRANSFER
Vol. 22, No. 4, October–December 2008

Characterizing High-Energy-Density Propellants for Space Propulsion Applications

Timothy S. Kokan*
Georgia Institute of Technology, Atlanta, Georgia 30332
John R. Olds†
SpaceWorks Engineering, Inc., Atlanta, Georgia 30338
and
Jerry M. Seitzman‡ and Peter J. Ludovice§
Georgia Institute of Technology,
Atlanta, Georgia 30332

DOI: 10.2514/1.31164

A technique for computationally determining the thermophysical properties of high-energy-density matter propellants is presented. High-energy-density matter compounds are of interest in the liquid rocket engine industry due to their high-density and high-energy content relative to existing industry-standard propellants. To accurately model rocket engine performance, cost, and weight in a conceptual design environment, several thermodynamic and physical properties are required over a range of temperatures and pressures. The approach presented here combines quantum mechanical and molecular dynamic calculations and group additivity methods. A method for improving the force field model coefficients used in the molecular dynamics simulations is included. This approach is used to determine thermophysical properties for two high-energy-density matter compounds of interest: quadricyclane and 2-azido-N, N-dimethylethanamine. The modified force field approach provides results that more accurately match experimental data than the unmodified approach. Launch vehicle and lunar lander case studies are presented to quantify the system-level impact of employing quadricyclane and 2-azido-N, N-dimethylethanamine rather than industry-standard propellants. In both cases, the use of high-energy-density matter propellants provides reductions in vehicle mass compared with industry-standard propellants. The results demonstrate that high-energy-density matter propellants can be an attractive technology for future launch vehicle and lunar lander applications.

I. Introduction

THERE is an extensive interest in high-energy-density matter (HEDM) propellants as potential replacements for industry-standard fuels [liquid hydrogen (LH2), refined petroleum-1 or rocket propellant-1 (RP-1), monomethyl hydrazine (MMH), and unsymmetrical dimethylhydrazine] for liquid rocket engines. The synthesis and development of HEDM propellants has been investigated by the U.S. Air Force Research Laboratory [1,2], the U.S. Army Research Laboratory [3,4], the NASA Marshall Space Flight Center [5], and the NASA John H. Glenn Research Center at Lewis Field [6,7].

Most conceptual rocket engine powerhead design tools (e.g., NPSS, ROCETS, and REDTOP-2) require several thermophysical properties of a given propellant in order to perform conceptual vehicle designs. These properties include enthalpy, entropy, density, kinematic viscosity, and thermal conductivity [8–10]. For most of the potential new HEDM propellants, these thermophysical data either do not exist or are incomplete over the range of temperatures and pressures necessary for liquid rocket engine design and analysis.

Received 1 May 2007; accepted for publication 2 May 2008.

*Graduate Research Assistant, School of Aerospace Engineering, 270 Ferst Drive. Student Member AIAA.
†Chief Executive Officer, 1200 Ashwood Parkway, Suite 506. Associate Fellow AIAA.
‡Associate Professor, School of Aerospace Engineering, 270 Ferst Drive. Associate Fellow AIAA.
§Associate Professor, School of Chemical and Biomolecular Engineering, 311 Ferst Drive.

Therefore, if one wishes to use HEDM propellants in a conceptual vehicle design, a technique for determining their thermophysical properties in a quick and efficient manner must be employed. Current computational techniques, such as molecular dynamics, cannot model complex HEDM molecules to the level of accuracy needed for rocket engine powerhead design tools without modification of the molecular dynamics force field equation parameters [3,4]. Molecular dynamics (MD) simulations, by modeling the intra- and intermolecular motions and distributions of molecules, can provide predictions of the enthalpy, entropy, and density of substances as a function of temperature and pressure [11]. Molecular dynamics simulations make use of force field equations to determine the energy potential between atoms and molecules. These force field equations model the energy associated with bond length stretching, bond angle bending, and dihedral angle rotation within a molecule, as well as the electrostatic and van der Waals energies between molecules. The force field model developed by Sun [12], called the condensed-phase optimized molecular potentials for atomistic simulation studies (COMPASS), has many advantages for MD simulations. It is a molecular force field model that has been optimized for condensed phases [12–15]. Thus, it is particularly useful for predicting thermophysical properties for rocket propellants, because the propellant is normally in a condensed phase for the majority of the time it flows through the different engine components. In addition, the COMPASS force field model has been shown to be useful in predicting energies and densities of a variety of simple hydrocarbon molecules. It is important to note, however, that the coefficients in the model were optimized to predict the properties of these various alkanes, alkenes, and alkynes [12,13]. The COMPASS model has not been used for more complex strained-bond hydrocarbons that are typical in proposed HEDM propellants. Therefore, it is expected that the COMPASS model coefficients will have to be modified for HEDM-type molecules.

This property prediction technique is validated via a series of verification experiments of HEDM compounds. Results are provided

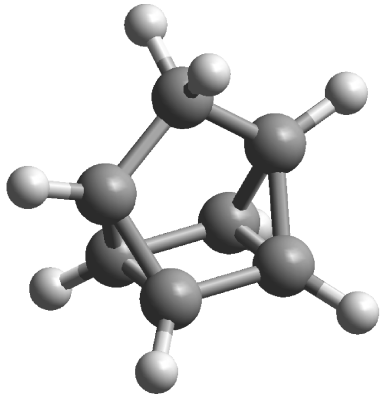

Fig. 1 Ball and cylinder rendering of quadricyclane (C_7H_8).

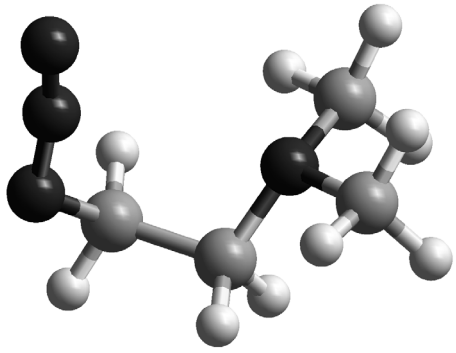

Fig. 2 Ball and cylinder rendering of DMAZ ($C_4H_{10}N_4$).

for two HEDM propellants: quadricyclane and 2-azido-N, N-dimethylethanamine (DMAZ). Ball and cylinder models of quadricyclane and DMAZ are shown in Figs. 1 and 2. Both quadricyclane and DMAZ are liquids at standard temperature and pressure. The calculated thermophysical properties are compared against experimental measurements. Furthermore, the thermophysical property results are used to examine the conceptual design of two vehicles. The first case study is the lunar lander ascent stage of NASA's proposed lunar Exploration Systems Architecture Study (ESAS). The second case study is the booster stage of the Lockheed Martin Atlas V 402 launch vehicle. The goal of these studies is to help quantify the weight and performance benefits of using quadricyclane or DMAZ over existing industry-standard hydrocarbon fuels for space propulsion applications.

II. Analysis Technique

The method used to calculate the HEDM thermophysical properties consists of three main steps. First, quantum mechanical energy calculations are used to determine the kinetic energy and intramolecular potential energy of the compound of interest as a function of temperature. Second, molecular dynamics simulations are used to determine the density, enthalpy change, and entropy change of the compound of interest at a range of temperatures and pressures. Third, additivity methods are used to determine the kinematic viscosity and thermal conductivity of the compound of interest over the same temperature and pressure ranges. For an unknown material, the three steps involved in this method can typically be performed by a working engineer within one week, including computational time. The methods are described in some detail here; further details are available in [16].

As noted already, the COMPASS force field model [12] was chosen for the molecular dynamic simulations. However, as the coefficients in the model were optimized to predict the properties of simpler hydrocarbon molecules, it is anticipated that the model will require modification to accurately handle HEDM propellants. The COMPASS force field model modifications are made by comparing thermophysical properties predicted from molecular dynamics simulations with experimental data for model substances. The COMPASS force field model parameters are adjusted in order to minimize the difference between the predicted and measured properties. Because of the fact that little or no experimental data exist for the HEDM propellants, model compounds for which the properties are known are used to determine the best settings for the COMPASS force field parameters. Model compounds are those compounds that have a molecular structure similar to the HEDM propellant of interest and have published thermophysical data available for use.

The property calculation method starts with an initial molecular configuration of the HEDM compound and corresponding model compound. These molecular configurations are provided either from published data or from quantum mechanical energy minimization. A method developed by Lagache et al. [17] and Cadena et al. [18,19] is used to determine the enthalpy and specific heat of the liquid HEDM and model compounds as a function of temperature and pressure. This method breaks down the calculation of enthalpy (and specific heat) into ideal-gas and residual components, as shown in Eq. (1):

$$c_p(T,P) = c_p^{\text{ig}}(T) - R + c_p^{\text{res}}(T,P) \tag{1}$$

where T is temperature, P is pressure, $c_p^{\text{ig}}(T)$ is the ideal-gas component of the specific heat, and $c_p^{\text{res}}(T,P)$ is the residual component. The ideal-gas component is calculated through the use of quantum mechanically calculated normal-mode vibrational frequencies. The residual component is determined through molecular dynamics simulation.

A. Quantum Mechanics

A quantum mechanical vibrational analysis is performed in order to calculate the vibrational normal-mode frequencies of the molecule of interest using the general atomic and molecular electronic structure system (GAMESS) [20]. The resulting harmonic vibrational frequencies are scaled to account for anharmonic effects [21]. With these vibrational frequencies, one can calculate the ideal-gas specific heat. The following equations are used for a nonlinear molecule:

$$c_p^{\text{ig}}(T) - R = c_v^{\text{tr}} + c_v^{\text{rot}} + c_v^{\text{vib}} \tag{2}$$

$$c_v^{\text{tr}} = c_v^{\text{rot}} = \tfrac{3}{2}R \tag{3}$$

$$c_v^{\text{vib}}(T) = \sum_{i=1}^{3N-6} R\left(\frac{\theta_{\text{vib}_i}}{T}\right)^2 \frac{e^{\theta_{\text{vib}_i}/T}}{(e^{\theta_{\text{vib}_i}/T}-1)^2} \tag{4}$$

$$\theta_{\text{vib}_i} = \frac{h\nu_i}{k_B} \tag{5}$$

In Eq. (2), R is the universal gas constant, and c_v^{tr}, c_v^{rot}, and c_v^{vib} are, respectively, the translational, rotational, and vibrational components of the specific heat at constant volume. In Eq. (4), N is the number of atoms in the molecule, and θ_{vib_i} is the characteristic vibrational temperature of the ith vibrational normal mode. In Eq. (5), h is Planck's constant, k_B is Boltzmann's constant, and ν_i is the ith normal-mode vibrational frequency found from quantum mechanical analysis.

Using Eq. (2), one can calculate the ideal-gas specific heat as a function of temperature for a molecule of interest. Ideal-gas sensible enthalpy (less RT) is calculated by integrating the ideal-gas specific heat in the following manner:

$$h_{\text{sensible}}^{\text{ig}} - RT = \int_{298.15\ \text{K}}^{T} c_p^{\text{ig}}(\tau)\,\mathrm{d}\tau - RT \tag{6}$$

B. Molecular Dynamics

As noted previously, the COMPASS model is used in the molecular dynamics simulations. This force field model is detailed in Eq. (7). The molecular dynamics simulations are used for two purposes: 1) determination of the optimized values for the intermolecular parameters of the COMPASS force field model [last term in Eq. (7)] and 2) calculation of the enthalpy, entropy, and density of the HEDM molecule of interest over the range of temperatures and pressures experienced in a liquid rocket engine. Figure 3 shows a snapshot of a molecular dynamics simulation of one such potential rocket propellant and HEDM molecule, liquid DMAZ.

$$
\begin{aligned}
E^{\text{COMPASS}} &= \sum_{b}[k_2(b-b_0)^2 + k_3(b-b_0)^3 + k_4(b-b_0)^4] \\
&+ \sum_{\theta}[h_2(\theta-\theta_0)^2 + h_3(\theta-\theta_0)^3 + h_4(\theta-\theta_0)^4] \\
&+ \sum_{\phi}[V_1(1-\cos\phi) + V_2(1-\cos 2\phi) + V_3(1-\cos 3\phi)] \\
&+ \sum_{\chi}K_{\chi}(\chi-\chi_0)^2 + \sum_{b,b'}K_{bb'}(b-b_0)(b'-b'_0) \\
&+ \sum_{\theta,\theta'}K_{\theta\theta'}(\theta-\theta_0)(\theta'-\theta'_0) + \sum_{b,\theta}K_{b\theta}(b-b_0)(\theta-\theta_0) \\
&+ \sum_{b,\phi}(b-b_0)[G_1\cos\phi + G_2\cos 2\phi + G_3\cos 3\phi] \\
&+ \sum_{\theta,\phi}(\theta-\theta_0)[F_1\cos\phi + F_2\cos 2\phi + F_3\cos 3\phi] \\
&+ \sum_{\theta,\theta',\phi}K_{\theta\theta'\phi}(\theta-\theta_0)(\theta'-\theta'_0)\cos\phi + \sum_{i,j}\frac{q_iq_j}{r_{ij}} \\
&+ \sum_{i,j}\varepsilon_{ij}\left[2\left(\frac{\sigma_{ij}}{r_{ij}}\right)^9 - 3\left(\frac{\sigma_{ij}}{r_{ij}}\right)^6\right] \qquad (7)
\end{aligned}
$$

Molecular dynamics is used in conjunction with experimental data to determine the intermolecular parameter values. These terms describe the intermolecular potential (the potential between two atoms in different molecules or two atoms in the same molecule not connected through a bond, angle, or dihedral). With little or no experimental data available for the HEDM propellants, a model compound is used in this step of the method. By model compound, we mean a substance that has a molecular structure (i.e., atom groups, atom types, and bond structure) similar to the HEDM compound and also has available experimental thermophysical data. The model compounds chosen for DMAZ and quadricyclane are ethyl azide (see Fig. 4) and norbornane (see Fig. 5).

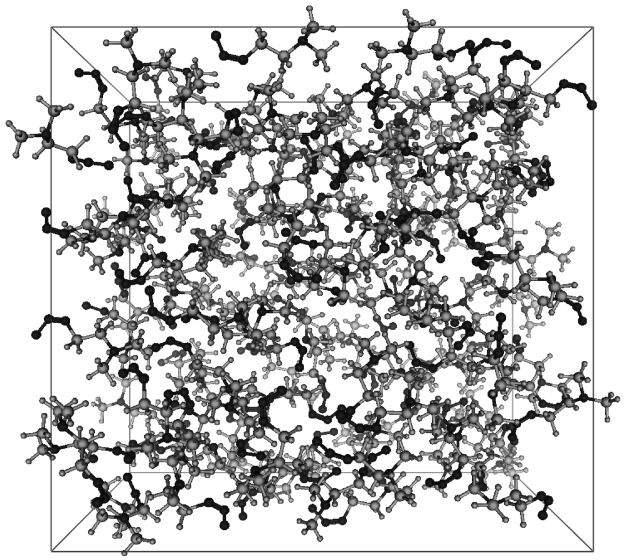

Fig. 3 Molecular dynamics snapshot of liquid DMAZ simulation.

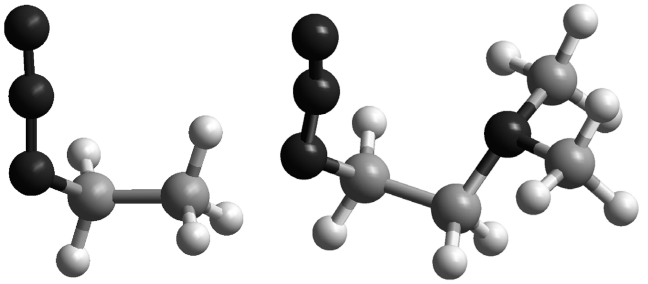

a) b)

Fig. 4 Ball and cylinder renderings of a) ethyl azide ($C_2H_5N_3$) and b) DMAZ ($C_4H_{10}N_4$).

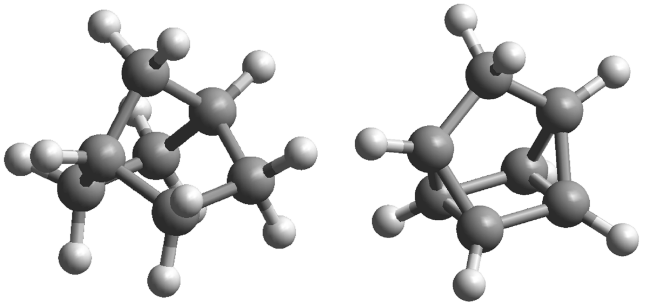

a) b)

Fig. 5 Ball and cylinder renderings of a) norbornane (C_7H_{12}) and b) quadricyclane (C_7H_8).

1. *Fitting Intermolecular Parameters*

The intermolecular parameters shown in the last term of Eq. (7) (σ and ε for the different types of atoms) are adjusted to improve the accuracy of the molecular dynamics simulations at predicting density and specific heat. A design of experiments is performed on the intermolecular parameters to determine the sensitivity of density and specific heat to changes in these parameters. A central composite design is the design of experiments chosen for this work. For norbornane, there are six intermolecular parameters that are adjusted: ε and σ for each atom type. There are three atom types: 1) a carbon atom attached to two or fewer heavy atoms, 2) a carbon atom attached to three or more heavy atoms, and 3) a hydrogen atom. With six design variables, the central composite design requires 47 runs (including three center points) for each temperature and pressure combination of interest. That is, 47 molecular dynamics runs are required to sufficiently model the sensitivity of density to the six intermolecular parameters. Specific-heat sensitivities are modeled in a similar manner. The same process is used for ethyl azide, with a different set of intermolecular parameters of interest.

Two response surface equations (RSEs) are created for each model compound to relate the predicted density and predicted c_p from the molecular dynamic simulations to the settings for the intermolecular parameters. These RSEs, which are simply multidimensional curve fits, are fit to the molecular dynamics design of experiments runs. The RSE chosen includes the first-order and second-order main effects plus all second-order cross terms. For the six-design-variable norbornane example, this results in 28 coefficients that must be fit to create the response surface.

Once the RSEs for density and specific heat are created, the intermolecular variable values are optimized. The goal of the optimization is to match the RSE-predicted density and specific-heat values with experimental results. Validation molecular dynamics runs are then performed using the optimized parameters to verify that the predicted thermophysical values from the response surface match the molecular dynamics results.

2. Molecular Dynamics Thermophysical Property Calculations

Molecular dynamics are used to compute the equilibrium properties of both the model compound and the HEDM compound at a range of temperatures and pressures [11,22]. This is done by expressing these equilibrium properties as a function of the positions and momenta of the particles in the system. The first observable that is defined is the kinetic energy per particle. For a system of point masses, the average kinetic energy of the system is defined using Eq. (8):

$$E_{\text{kin}} = \frac{1}{2}\sum_{i=1}^{N} m_i(\vec{v}_i \cdot \vec{v}_i) \tag{8}$$

where N is the number of particles in the system, and m_i and $\vec{v}_i$ are the respective mass and velocity of particle i. In the case of polyatomic molecules, m_i is the mass of the molecule and the velocity of the center of mass of the molecule. From this definition of kinetic energy, the average translational temperature of the system of particles (in three-dimensional space) can be defined using Eq. (9):

$$T_{\text{trans}} = \frac{2E_{\text{kin}}}{3Nk_B} = \frac{1}{3Nk_B}\sum_{i=1}^{N} m_i(\vec{v}_i \cdot \vec{v}_i) = \frac{2}{3k_B}\left(\frac{1}{2N}\sum_{i=1}^{N} m_i(\vec{v}_i \cdot \vec{v}_i)\right) \tag{9}$$

where k_B is Boltzmann's constant. With the translational temperature defined, the pressure can then be defined using Eq. (10):

$$P = \frac{Nk_BT_{\text{trans}}}{V} + \frac{1}{3V}\sum_{i=1}^{N-1}\sum_{j=i+1}^{N}\sum_{\alpha=1}^{n}\sum_{\beta=1}^{n} \vec{f}_{ij}^{\alpha\beta} \cdot \vec{r}_{ij}^{\alpha\beta} \tag{10}$$

where V is the volume of the computational space, $\vec{f}_{ij}^{\alpha\beta}$ is the force vector of atom β of molecule j on atom α of molecule i, and $\vec{r}_{ij}^{\alpha\beta}$ is the position vector from atom β of molecule j to atom α of molecule i. The first term of Eq. (10) is the ideal-gas term and the second term is the configurational or virial term that becomes prominent at higher densities (farther away from the ideal-gas assumption). Density is defined in Eq. (11) as

$$\rho = \frac{N}{V}\sum_{i=1}^{N} m_i \tag{11}$$

With these fundamental properties defined as a function of the positions and momenta of the particles, more complex equilibrium properties can also be defined. For example, the definition of enthalpy begins by dividing it into three components: enthalpy of formation, ideal-gas sensible enthalpy, and residual sensible enthalpy:

$$h(T,P) = \Delta h_f^0 + h_{\text{sens}}^{\text{ig}}(T) + h_{\text{sens}}^{\text{res}}(T,P) \tag{12}$$

$$h_{\text{sens}}^{\text{res}}(T,P) = \left[E_{\text{inter}}(T,P) + \frac{P}{\rho}\right] - \left[E_{\text{inter}}(T_0,P_0) + \frac{P_0}{\rho_0}\right] \tag{13}$$

$$E_{\text{inter}}(T,P) = E_{\text{vdwl}}(T,P) + E_{\text{coul}}(T,P) \tag{14}$$

In Eq. (12), the enthalpy of formation, Δh_f^0, is typically defined as the enthalpy of the substance at 298 K and 1 atm with respect to the arbitrary basis elements that make up that particle at the same temperature and pressure [23]. The second and third terms in Eq. (12) are defined using the method developed by Lagache [17] and Cadena et al. [18,19] for calculating the enthalpy of a liquid substance using quantum mechanics and molecular dynamics. The second term, $h_{\text{sens}}^{\text{ig}}$, is the ideal-gas sensible enthalpy defined previously in Eq. (6). The ideal-gas sensible enthalpy is based upon the normal-mode vibrational frequencies found from quantum mechanical analysis. The third term in Eq. (12), the residual sensible enthalpy, $h_{\text{sens}}^{\text{res}}$, represents the condensed-phase influence on the sensible enthalpy. This term, found from molecular dynamics simulations, is based upon the intermolecular energy (van der Waals and Coulomb) and the pressure divided by the density.

The second equilibrium property defined is entropy. Entropy can be defined similarly to enthalpy by breaking up entropy into its two major components, entropy of formation and sensible entropy:

$$s(T,P) = \Delta s_f^{1\text{ atm}} + s_{\text{sens}}(T,P) \tag{15}$$

The entropy of formation, $\Delta s_f^{1\text{ atm}}$, is typically defined as the entropy of the substance at 298 K and 1 atm. The entropy of a substance is normally defined to be zero at a temperature of absolute zero. The second term, s_{sens}, is known as the sensible entropy and is defined as the difference in entropy between any given state and the state at which the formation entropy is defined. The entropy of formation of the molecule of interest is taken from the quantum mechanics energy calculation code GAMESS. The sensible entropy for a simple compressible substance is defined with a form of Gibb's equation [23]:

$$\mathrm{d}s = \frac{\mathrm{d}h}{T} - \frac{\mathrm{d}P}{\rho T} = \left[\frac{\partial h/\partial T|_P}{T}\right]\mathrm{d}T + \left[\frac{\partial h/\partial P|_T}{T} - \frac{1}{\rho T}\right]\mathrm{d}P \tag{16}$$

Because the change in entropy from one state to another is path independent, one can define $s_{\text{sens}}(T_1,P_1)$ as

$$s_{\text{sens}}(T_1,P_1) = [s(T_1,P_0) - s(T_0,P_0)] + [s(T_1,P_1) - s(T_1,P_0)] \tag{17}$$

where T_0 and P_0 are the temperature and pressure at which the entropy of formation is defined (298 K and 1 atm) and $s(T_0,P_0)$ is the entropy of formation, $\Delta s_f^{1\text{ atm}}$. Figure 6 is a graphical representation of the process used for calculating sensible entropy: the entropy change from the formation conditions (T_0 and P_0) is determined with a combination of a constant-pressure simulation (to T_1 and P_0) and a constant-temperature process (to T_1 and P_1).

Thus, we have

$$\begin{aligned} s(T_1,P_1) - s(T_0,P_0) &= \int_{T_0}^{T_1}\left[\frac{\partial h/\partial T|_P}{T}\right]\mathrm{d}T \\ &+ \int_{P_0}^{P_1}\left[\frac{\partial h/\partial P|_T}{T_1} - \frac{1}{\rho(T_1,P)T_1}\right]\mathrm{d}P = \int_{T_0}^{T_1}\frac{c_p(T,P_0)}{T}\,\mathrm{d}T \\ &+ \int_{P_0}^{P_1}\left[\frac{\partial h/\partial P|_T}{T_1} - \frac{1}{\rho(T_1,P)T_1}\right]\mathrm{d}P \end{aligned} \tag{18}$$

The integrals can be numerically integrated from the MD results for enthalpy to calculate the total entropy as a function of temperature

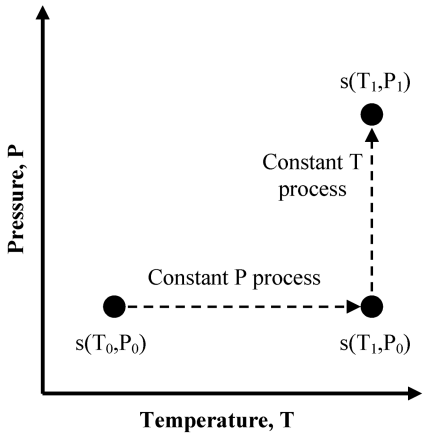

Fig. 6 Schematic of process used for calculating entropy change using MD results.

and pressure in order to create property data tables for rocket engine design codes.

C. Additivity Methods

Additivity methods are used to compute the kinematic viscosity and thermal conductivity of the propellants of interest. Additivity methods are used instead of molecular dynamics, because kinematic viscosity and thermal conductivity have less of an affect on the engine parameters of interest (specific impulse, engine weight) than do density, enthalpy, and entropy [16]. As a result, a less accurate, but less time-consuming and less computationally expensive, method can be used.

Additivity methods make use of the observation that a substance's physical properties depend on that substance's particular molecular structure [24,25]. In 1958 Benson and Buss [26] showed that it was possible to make a system of *additivity rules* to determine certain thermodynamic and physical properties of substances based upon their atom, bond, and group makeup. Individual contributions from atoms, bonds, and groups to the estimated values of thermophysical properties can be calculated by regressing empirical thermophysical data for known substances. For this work, the additivity parameter method developed by Chung et al. [27] is used for its ability to handle many different molecules over a wide range of temperatures and pressures. This method can be implemented in a spreadsheet and the calculations can be performed very rapidly.

D. Experimental Methods

In general application of this thermophysical parameter calculation method, little or no experimental testing is needed. This is because the method uses previously published experimental data from model compounds to determine the appropriate settings for the intermolecular potential parameters.

For this research, however, validation of the computational results from the quantum mechanical, molecular dynamics, and group additivity-method analyses is necessary. For future use, it is assumed that validation of the computation-based method is not required. Only validation with a new compound of interest's corresponding model compound is required. Experimental data for quadricyclane were previously published by Wucherer and Wilson [1]. However, very little published experimental data exist for the other HEDM compound of interest, DMAZ. As a result, experimental testing of DMAZ was performed as part of this research work. A sample of DMAZ was obtained from MACH I, Inc., a 3M distributor.

Experimental data at relatively low temperatures ($T < 450$ K) and pressures ($P < 20$ atm) were obtained in laboratories in the School of Chemical and Biomolecular Engineering and in the School of Materials Science and Engineering at Georgia Institute of Technology. American Society for Testing and Materials standard testing procedures were followed in all cases except for the measurement of thermal conductivity. Thermal conductivity was measured using a testing procedure developed by Bleazard [28]. The results of these experimental measurements are provided in the following section.

Table 1 Ethyl azide optimized intermolecular parameters

Intermolecular parameter	x_i	Baseline COMPASS value	Optimized value
σ_{n1z}	0.982	3.520	3.457
ε_{n1z}	1.013	0.085	0.086
σ_{n2t}	1.001	3.300	3.303
ε_{n2t}	0.854	0.050	0.043
σ_{n2z}	1.176	3.400	3.997
ε_{n2z}	1.075	0.120	0.129
σ_{c4z}	1.050	3.650	3.831
ε_{c4z}	1.009	0.080	0.081
σ_{h1}	1.018	2.878	2.931
ε_{h1}	1.002	0.023	0.023

Table 2 Norbornane optimized intermolecular parameters

Intermolecular parameter	x_i	Baseline COMPASS value	Optimized value
σ_{c4}	1.090	3.854	4.200
ε_{c4}	1.469	0.062	0.091
σ_{c43}	0.945	3.854	3.641
ε_{c43}	1.433	0.040	0.057
σ_{h1}	0.797	2.878	2.295
ε_{h1}	1.180	0.023	0.027

III. Results

A. Property Calculations

Using the process described in Sec. II, the intermolecular potential parameters [used in Eq. (7)] for both ethyl azide and norbornane were optimized. The results are provided in Tables 1 and 2. In these tables, the σ_i have units of angstroms (Å) and the ε_i have units of kcal/mol.

With the optimized values for the intermolecular parameters determined, these values can then be used in the prediction of the thermophysical properties of each model compound's corresponding HEDM compound. The results of these molecular dynamics simulations are provided in Figs. 7–12. Both the baseline COMPASS model simulations (those using the published baseline COMPASS intermolecular parameter values) and the optimized intermolecular parameter simulations are provided. As shown subsequently, the optimization with model compounds can provide significant improvements in the predictive accuracy of the MD simulations.

The experimental measurements and corresponding molecular dynamics simulations for DMAZ were performed for a range of

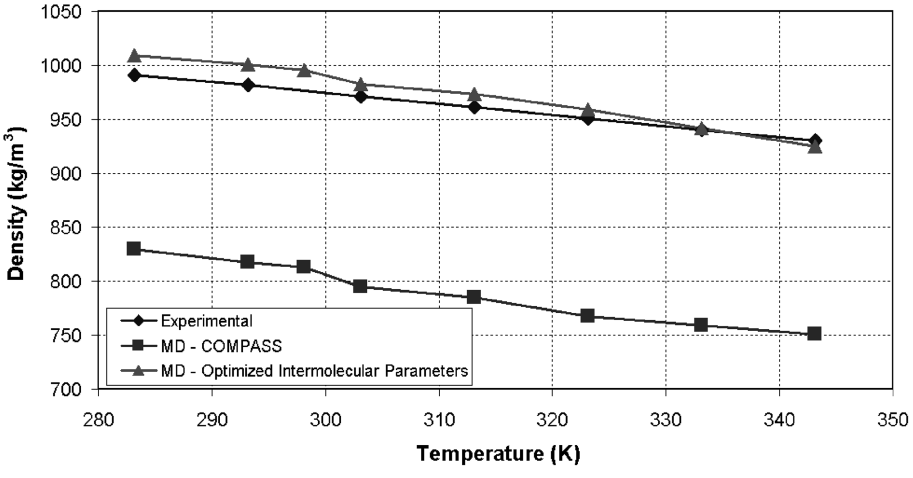

Fig. 7 Quadricyclane density as a function of temperature ($P = 1$ atm).

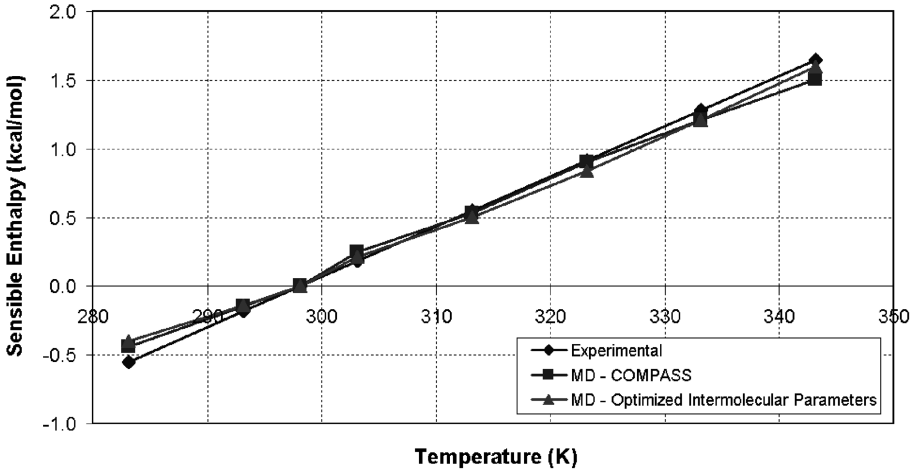

Fig. 8 Quadricyclane sensible enthalpy as a function of temperature ($P = 1$ atm).

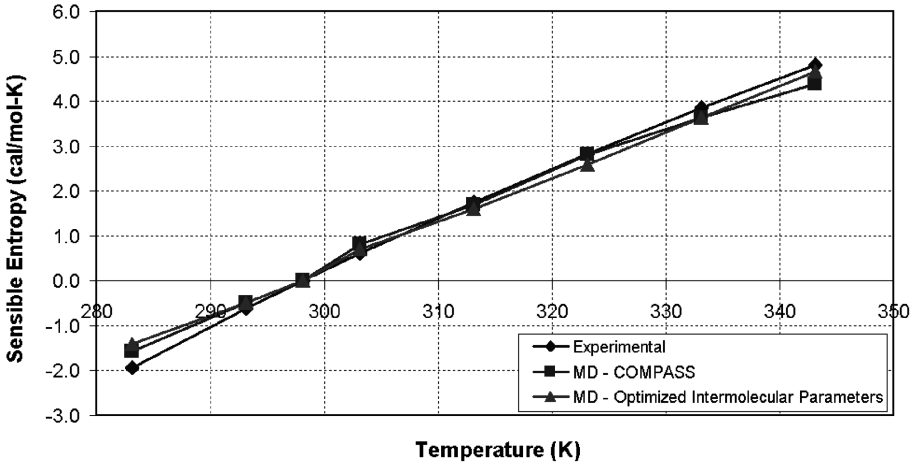

Fig. 9 Quadricyclane sensible entropy variation with temperature ($P = 1$ atm).

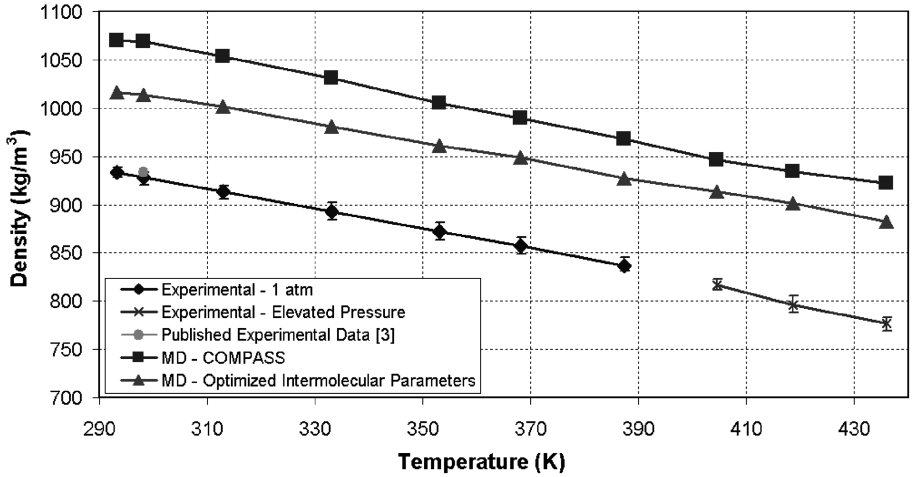

Fig. 10 DMAZ density variation with temperature.

pressures. The experimental measurements of DMAZ at the three highest temperatures were performed at elevated pressures in order to suppress boiling. Minimum and maximum bars are provided for the DMAZ experimental measurements. A previously published data point (from [3]) for the density of DMAZ at 298 K is provided in Fig. 10 for reference.

The rms deviations of both the baseline COMPASS simulations and optimized intermolecular parameter simulations are provided in Table 3. The deviations in total enthalpy and entropy are calculated by adding the sensible components shown in the preceding figures to the enthalpy and entropy of formation of each compound. The enthalpy and entropy of formation of each HEDM compound is provided in Table 4.

As can be seen from Table 3, the rms deviations in density for both quadricyclane and DMAZ are reduced through the optimization of the molecular dynamics intermolecular potential function

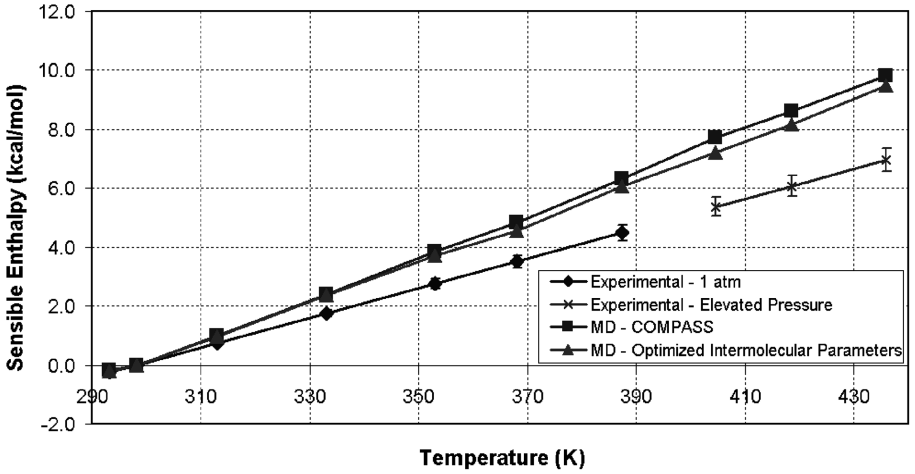

Fig. 11 DMAZ sensible enthalpy as a function of temperature.

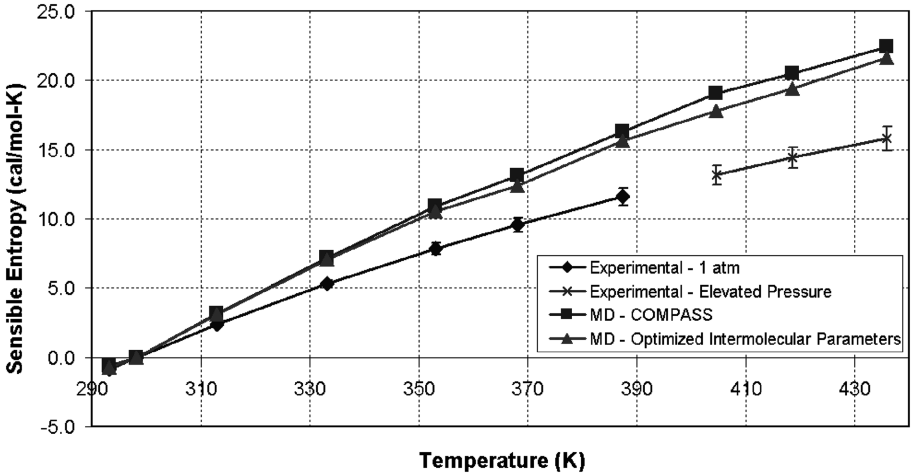

Fig. 12 DMAZ sensible entropy variation with temperature.

parameters. A greater improvement is shown with quadricyclane than with DMAZ. This is most likely due to three causes: 1) the lack of changes made to the charge bond parameters (the charge bond parameters for the nitrogen bonds in DMAZ are much larger than those for the carbon bonds in quadricyclane), 2) the choice of model compound, and 3) the quality of model compound density RSE.

The rms deviations in total enthalpy and total entropy for quadricyclane are very small for both the baseline COMPASS and optimized intermolecular simulations. The deviations in specific heat for quadricyclane are reduced through the optimization method. Specific heat is listed in addition to enthalpy and entropy, because it is a good indication of the accuracy in predicting the changes in these thermodynamic properties as a function of temperature and pressure.

Table 3 RMS deviations (from experimental data) of molecular dynamics property predictions

	COMPASS rms deviation	Optimized intermolecular parameters rms deviation
Quadricyclane		
Density	18.20%	1.12%
Total enthalpy	0.08%	0.08%
Total entropy	0.43%	0.46%
c_p	11.39%	9.00%
DMAZ		
Density	15.95%	10.95%
Total enthalpy	1.80%	1.51%
Total entropy	6.73%	5.67%
c_p	36.86%	32.45%

In rocket engine powerhead design, the total enthalpy is used in the combustion analysis, but only the change in entropy is used.

The deviations for DMAZ are higher than those for quadricyclane. As a result, there is greater room for improvement in the predictive accuracy of the molecular dynamics simulations for DMAZ than for quadricyclane. Although improved accuracy is achieved for DMAZ, there is still room for further improvement in the areas outlined previously (charge bond parameters, choice of model compound, and quality of model compound RSEs).

Using the density predictions from the MD simulations and the definition of the molecule (atoms, bonds, and groups), additivity methods were used to predict the kinematic viscosity and thermal conductivity of each HEDM compound as a function of temperature and pressure. The results are provided in Figs. 13–16.

Similar to the DMAZ thermodynamic property results, the experimental measurements and corresponding additivity-method calculations were performed for a range of pressures. The experimental measurements of DMAZ at the three highest temperatures were performed at elevated pressures in order to suppress boiling. Minimum and maximum bars are provided for the DMAZ experimental measurements.

Table 4 HEDM compound enthalpy and entropy of formation

HEDM compound	Δh_f^0, kcal/mol	$\Delta s_f^{1\,\text{atm}}$, cal/mol · K
Quadricyclane	72.2 [29]	39.9 [29]
DMAZ	66.9 [30]	36.8 [30]

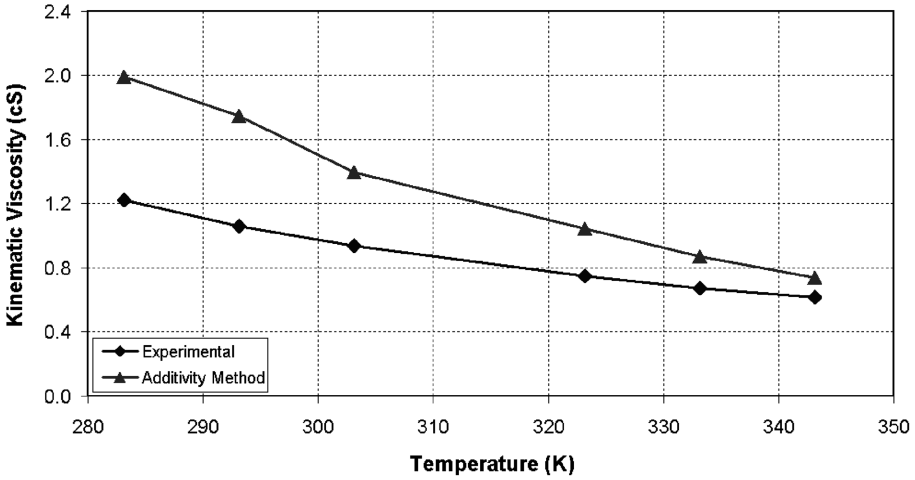

Fig. 13 Quadricyclane kinematic viscosity as a function of Temperature ($P = 1$ atm).

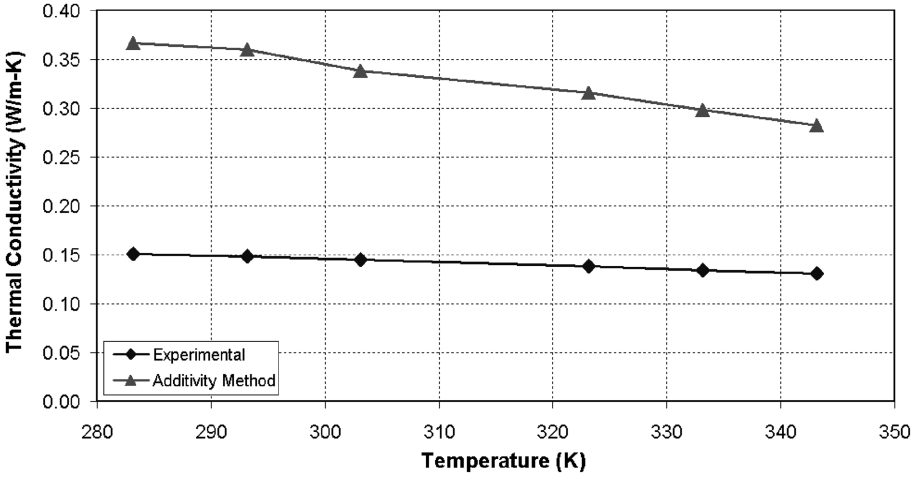

Fig. 14 Quadricyclane thermal conductivity as a function of temperature ($P = 1$ atm).

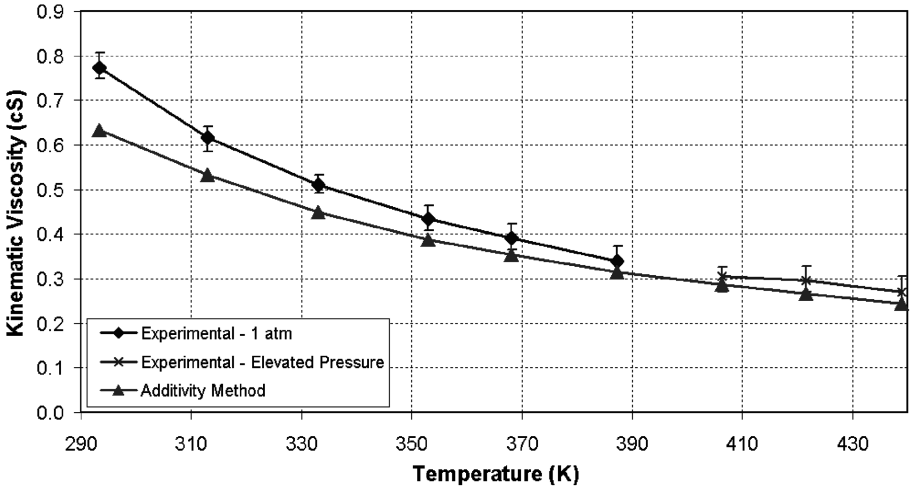

Fig. 15 DMAZ kinematic viscosity as a function of temperature.

The average rms deviations of the additivity-method calculations are provided in Table 5. The deviations for viscosity and thermal conductivity are much larger than for density, enthalpy, and entropy; however, this should not have a significant impact on rocket engine powerhead design, because the sensitivity of I_{sp} to changes/errors in these parameters is very small. Even an error greater than 100%, such as that seen in the thermal conductivity of quadricyclane, has a minimal impact on I_{sp} [16]. If greater accuracy is needed in the prediction of these properties, other calculation techniques such as molecular dynamics could be employed.

With the thermophysical properties for quadricyclane and DMAZ validated to the level of accuracy needed for rocket engine powerhead design codes, propellant property data tables can be created for use in rocket engine powerhead design.

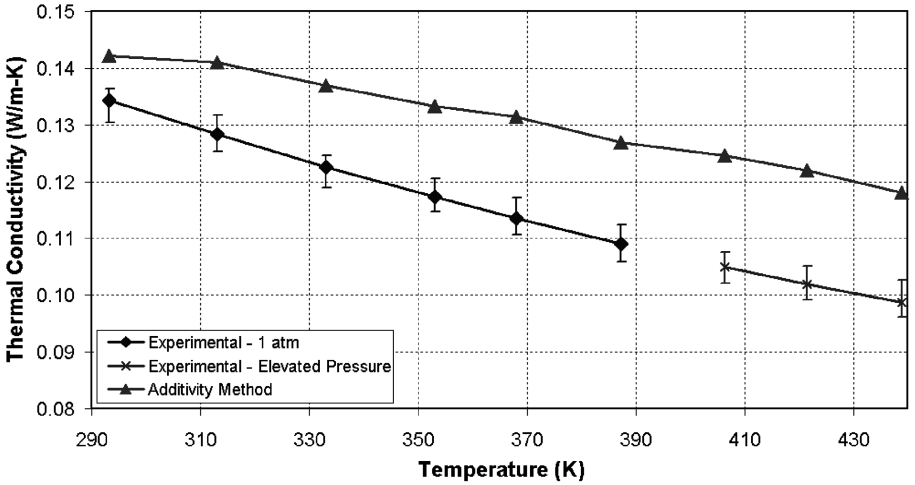

Fig. 16 DMAZ thermal conductivity as a function of temperature.

B. Case Studies

Two conceptual vehicle design case studies are performed using the calculated DMAZ and quadricyclane thermophysical properties. The first case study is the Lunar Surface Access Module (LSAM) used in the NASA Exploration Systems Architecture Study (ESAS) [31]. The second case study is the Lockheed Martin Atlas V 402 launch vehicle.

A sensitivity of engine and vehicle performance to variation in thermophysical properties is performed to quantify the effect of differences between predicted and experimental properties on engine I_{sp} and vehicle payload mass. The results of this sensitivity are shown in Table 6 through the use of the ROCETS powerhead design code [10]. The results in Table 6 show that the variation in vacuum I_{sp} as total enthalpy, total entropy, density, kinematic viscosity, and thermal conductivity are each altered by 20%. Using the variation in calculated thermophysical properties with respect to the experiment, found in Tables 3 and 5, Table 7 provides the variation in vacuum I_{sp} to variations in thermophysical properties for both quadricyclane and DMAZ.

As can be seen in Table 7, the variations in thermophysical properties for both DMAZ and quadricyclane result in small variations in vacuum I_{sp}. The largest variations in vacuum I_{sp} are found from variations in total entropy (0.43%) and density (0.50%) of DMAZ. A 0.5% variation in vacuum I_{sp} for DMAZ translates into 1.8 s. A 1.8 s variation in vacuum I_{sp} results in a 1.7% variation in predicted payload for the Atlas V 402.

Table 5 Additivity-method average rms deviation

	Additivity-method average rms deviation
Quadricyclane	
Kinematic viscosity	45.64%
Thermal conductivity	129.73%
DMAZ	
Kinematic viscosity	10.81%
Thermal conductivity	14.59%

1. *Case Study 1: LSAM*

The LSAM is chosen for study because the propellant choice for the ascent stage of the LSAM is still undetermined. The current baseline propellant combination for the ascent stage is nitrogen tetroxide (NTO)–MMH. A propellant trade study was performed to compare the NTO–MMH baseline propellant combination with a currently proposed alternative of liquid oxygen (LOX)–methane and two HEDM propellant combinations: LOX–DMAZ and LOX–quadricyclane.

The ESAS final report [31] details the mission requirements for a crew plus cargo lunar mission [31]; an overview is provided in Table 8. An important requirement is that the LSAM be able to orbit the Earth for up to 120 days before beginning the mission. This allows several opportunities for the crew launch vehicle to launch and rendezvous with the orbiting cargo (including the LSAM). This requirement makes the LSAM propellant choices that much more important, because cryogenic propellant boiloff can be significant over such an extended period of time; cryogenic propellants will boil off during long-duration storage through environmental heating of the propellant tanks. As a result, extra propellant is needed to

Table 6 Thermophysical property sensitivity study

Enthalpy multiplier	Entropy multiplier	Density multiplier	Kinematic viscosity multiplier	Thermal conductivity multiplier	Vacuum I_{sp}, s
1.0	1.0	1.0	1.0	1.0	448.337
1.2	1.0	1.0	1.0	1.0	441.538
1.0	1.2	1.0	1.0	1.0	441.537
1.0	1.0	1.2	1.0	1.0	452.436
1.0	1.0	1.0	1.2	1.0	448.336
1.0	1.0	1.0	1.0	1.2	448.342

Table 7 Variation in vacuum I_{sp}

	Enthalpy	Entropy	Density	Kinematic viscosity	Thermal conductivity
Quadricyclane	0.006%	0.035%	0.055%	0.001%	0.007%
DMAZ	0.114%	0.430%	0.501%	0.000%	0.001%

Table 8 ESAS mission parameters

Parameter	Value
Number of crew	4
Payload to lunar surface	2395 kg
Mission time	7 days
On-orbit time	120 days
Dry weight margin	20%

accommodate these losses. This extra propellant also requires larger propellant tanks [32].

Two typical methods of minimizing propellant boiloff are insulation and cryocoolers. Typical cryogenic propellant tank insulation is a multilayer insulation (MLI) consisting of alternating layers of aluminized Mylar and Nomex [33,34]. Although insulation is advantageous because it requires no power to operate, it can typically only reduce propellant boiloff, not eliminate it. Cryocooler refrigeration systems, often based on Stirling or Brayton cycles, are used to maintain cryogenic temperatures [33]. Although cryocoolers can achieve zero boiloff when used in combination with insulation, they require power and can be fairly heavy. In this case study, both methods of propellant boiloff minimization are examined for the different propellant combinations.

A variety of discipline analysis codes were used in the conceptual vehicle analysis. The propulsion analysis is performed using REDTOP-2 [9], a powerhead design and analysis code that uses tabulated thermophysical propellant properties stored in text files. To incorporate the propellant data for quadricyclane and DMAZ, new data-table text files were created. The trajectory analysis was performed using the Program to Optimize Simulated Trajectories—3D (POST-3D) [35]. POST-3D is an industry-standard three-degree-of-freedom trajectory optimization code. The weights-and-sizing analysis was performed using industry-standard mass estimating relationships [36].

Results are presented in Table 9 for the four different propellant combinations (NTO–MMH, LOX–methane, LOX–DMAZ, and LOX–quadricyclane). The same cycle type (expander), expansion ratio (84), and chamber pressure (610 psi) are used for each engine. These choices are based upon the RL-10A-4 liquid rocket engine design [37]. This engine is chosen as a high-performance alternative to pressure-fed engines in order to produce a lighter-weight LSAM vehicle, allowing for a smaller cargo launch vehicle to be used to launch the LSAM and its associated Earth-departure stage into low Earth orbit (LEO). As can be seen from the last row in Table 9, the three alternative propellant combinations all have a higher I_{sp} than the NTO–MMH baseline.

Tables 10 and 11 are the mass results for the baseline propellant combination and the three propellant alternatives with the two propellant boiloff minimization methods. From a performance point of view, the three alternatives to the current NTO–MMH design all hold potential for overall LSAM gross mass savings. In both cases (MLI and MLI with a cryocooler), the alternative propellant combinations have a lower overall LSAM gross mass than the NTO–MMH baseline. In the case in which only MLI is used, the two HEDM alternatives provide more mass savings than the LOX–methane alternative. When MLI with cryocoolers are used (a more aggressive propellant boiloff minimization method), then the LOX–methane alternative becomes more attractive. This is because the LOX–methane alternative has both cryogenic fuel and oxidizers,

Table 9 Ascent stage engine comparison

	Baseline	Currently proposed alternative	HEDM alternative 1	HEDM alternative 2
Oxidizer	NTO	LOX	LOX	LOX
Fuel	MMH	Methane	Quadricyclane	DMAZ
Mixture ratio O/F	1.6	3.1	2.0	1.4
Cycle type	Expander	Expander	Expander	Expander
Expansion ratio ε	84	84	84	84
$P_{chamber}$, i	610	610	610	610
$\rho_{oxidizer}$, kg/m^3	1450	1141	1141	1141
ρ_{fuel}, kg/m^3	880	420	1025	1030
ρ_{bulk}, kg/m^3	1231	965	1102	1095
$T_{oxidizer}$, R	536.67	163	163	163
T_{fuel}, R	536.67	250	536.67	536.67
Engine thrust/weight	48.3	44.9	49.6	49.7
I_{sp}, s	330.35	365.97	357.43	354.77

Table 10 LSAM mass results comparison: MLI

	NTO–MMH	LOX–methane	LOX–quad	LOX–DMAZ
Ascent dry mass, kg	4660	4810	4690	4690
Ascent takeoff mass, kg	9580	9460	9330	9350
Descent dry mass,kg	5690	5670	5630	5630
Descent gross mass, kg	27,920	27,700	27,430	27,470
Ascent stage takeoff mass savings compared with baseline	0.00%	1.27%	2.67%	2.41%

Table 11 LSAM mass results comparison: MLI with cryocooler

	LOX–methane	LOX–quad	LOX–DMAZ
Ascent dry mass, kg	4730	4650	4650
Ascent takeoff mass, kg	9160	9140	9180
Descent dry mass, kg	5590	5580	5590
Descent gross mass, kg	27,120	27,070	27,140
Ascent stage takeoff mass savings compared with baseline	4.38%	4.58%	4.17%

whereas the two HEDM alternatives have only cryogenic oxidizers. As a result, the LOX–methane alternative is more sensitive to the type of boiloff minimization method used.

The LOX–quadricyclane alternative has the lowest LSAM gross weight for both boiloff minimization methods. This is due to a combination of high I_{sp} and high bulk density. Bulk density is defined as

$$\rho_{bulk} = \rho_{oxidizer} \times \frac{O/F}{O/F+1} + \rho_{fuel} \times \frac{1}{O/F+1} \tag{19}$$

where $\rho_{oxidizer}$ is the oxidizer density, ρ_{fuel} is the fuel density, and O/F is the oxidizer-to-fuel mixture ratio (by mass).

The LOX–quadricyclane I_{sp} and bulk density are both higher than for LOX–DMAZ. The LOX–quadricyclane I_{sp} is lower than that of LOX–methane, but the significantly higher bulk density more than makes up for the slightly lower I_{sp}. A high bulk density is desirable because it allows for smaller, lighter propellant tanks for the same propellant mass. These results indicate that the use of HEDM propellants may be an attractive option for the LSAM ascent stage engine. Further analysis including cost, operations, reliability, and safety should be done to further flush out the relative advantages and disadvantages of HEDM propellant combinations over NTO–MMH and LOX–methane. A significant advantage of the methods developed here is their ability to provide more accurate results for new propellants for which the thermophysical properties have not been adequately measured. It is common in such cases to employ a one-dimensional chemical equilibrium analysis code (for example, CEA [38] or REDTOP [39]) to estimate I_{sp}. These codes require the enthalpy of formation and storage density for the new propellant (e.g., measured or estimated). With this information, they typically provide results for ideal I_{sp} without losses. REDTOP is an exception: it uses an efficiency multiplier applied to the ideal I_{sp} to attempt to account for these losses. The multiplier is based upon regression of existing engine performance data, not on an engine component analysis. These efficiency multipliers, which depend upon the propellant type among other factors, are not generally applicable to new propellant combinations. Another drawback of these simplified codes is their inability to calculate the engine weight directly by estimating individual component weights. The engine thrust to weight is typically either an input or estimated from techniques such as that developed by Way and Olds [40].

Using this method for estimating engine thrust to weight and the chemical equilibrium analysis code REDTOP to predict I_{sp}, LSAM ascent and descent stages were designed. A comparison of engine results is provided for both REDTOP and REDTOP-2 in Table 12. The estimations for engine thrust to weight differ significantly between the two engine analysis codes. It is expected that the engine thrusts to weights from REDTOP-2 are more accurate because the analysis is based on an estimation of engine weight at the component level (turbopump, combustor, valves, propellant feed lines, etc.). The I_{sp} results from REDTOP are fairly close (between 1–5 s difference) to those from REDTOP-2 for the LOX–methane, LOX–quadricyclane, and LOX–DMAZ engines. However, the I_{sp} results are significantly different for the NTO–MMH engine (15.5 s difference). This is likely due to the fact that there is no expander cycle NTO–MMH data in the REDTOP database used to calculate engine efficiencies. Again assuming that the results from REDTOP-2 are more accurate, the results one could obtain without the thermophysical data provided by the MD simulation would produce an inaccurately large performance difference between the baseline NTO–MMH engine and the other three engines.

Tables 13 and 14 provide a comparison of the vehicle weight predictions using each engine analysis method. As expected from the previous analysis of engine I_{sp}, the baseline NTO–MMH combination has a larger weight difference compared with the

Table 12 Comparison of engine analysis code results

	NTO–MMH	LOX–methane	LOX–quad	LOX–DMAZ
REDTOP-2 powerhead design code				
Engine thrust/weight	48.3	44.9	49.6	49.7
I_{sp}, s	330.35	365.97	357.43	354.77
REDTOP chemical equilibrium code				
Engine thrust/weight	76.6	67.9	68.8	69.5
I_{sp}, s	314.81	361.38	355.51	353.74

Table 13 Comparison of vehicle results: MLI

	NTO–MMH	LOX–methane	LOX–quad	LOX–DMAZ
REDTOP-2 powerhead design code				
Ascent takeoff mass, kg	9580	9460	9330	9350
Descent gross mass, kg	27,920	27,700	27,430	27,470
Ascent stage takeoff mass savings compared with baseline	0.00%	1.27%	2.67%	2.41%
REDTOP chemical equilibrium code				
Ascent takeoff mass, kg	9800	9440	9290	9300
Descent gross mass, kg	28,350	27,670	27,350	27,380
Ascent stage takeoff mass savings compared with baseline	0.00%	3.72%	5.24%	5.09%

Table 14 Comparison of vehicle results: MLI with cryocooler

	LOX–methane	LOX–quad	LOX–DMAZ
REDTOP-2 powerhead design code			
Ascent takeoff mass, kg	9160	9140	9180
Descent gross mass, kg	27,120	27,070	27,140
Ascent stage takeoff mass savings compared with baseline	4.38%	4.58%	4.17%
REDTOP chemical equilibrium code			
Ascent takeoff mass, kg	9130	9100	9130
Descent gross mass, kg	27,060	26,980	27,040
Ascent stage takeoff mass savings compared with baseline	6.81%	7.14%	6.81%

alternative propellant combinations for the REDTOP analysis case. This is interpreted as an artificial penalization of the NTO–MMH combination due to a lower-fidelity engine analysis model. If one were making funding or design choices based upon a conceptual vehicle design analysis, one could be more inclined to investigate alternative propellant combinations for the LSAM ascent stage engine based upon the simplified results than upon the detailed approach made possible by the HEDM property predictions.

2. *Case Study 2: Atlas V 402*

The Atlas V is chosen for the second case study because it is the current state-of-the-art U.S. hydrocarbon-fueled launch vehicle. The Atlas V first stage uses a LOX/RP RD-180 engine. A sensitivity study of payload delivered to LEO as a function of propellant and mixture ratio was performed. Both quadricyclane and DMAZ were examined using two different scenarios.

Scenario 1 involves switching only the fuel from RP to one of the two HEDM propellants, while leaving all other aspects of the vehicle (tanks, primary structure, engine dimensions and operating conditions, and subsystems) the same as the baseline LOX/RP vehicle. In this scenario, the mixture ratio is adjusted by only partially filling one of the propellant tanks. For instance, using the Atlas V 402 propellant tanks, the LOX/quadricyclane mixture ratio is 2.24 with the tanks full. To increase this mixture ratio (increase the percentage of propellant that is oxidizer), the amount of quadricyclane is reduced, leaving a partially empty tank.

Scenario 2 involves adjusting the oxidizer and fuel-tank lengths in order to sweep over a wide range of mixture ratios while still keeping the launch vehicle dimensions, engine dimensions and operating conditions, and subsystems the same. In this scenario, the tanks can be completely filled with propellant.

As with the LSAM case study, a variety of discipline analysis codes were used. The propulsion and trajectory analyses again used REDTOP-2 and POST-3D. The weights-and-sizing analysis was based upon published weight breakdowns of the Atlas V [41]. The aerodynamics analysis was performed using the Aerodynamic Preliminary Analysis System [42]. The results of these analyses are shown in Figs. 17 and 18. The results are shown as a percentage change in payload to LEO versus the baseline LOX/RP Atlas V 402.

As can be seen from these results, quadricyclane is well suited as a potential fuel replacement for the Atlas V 402, whereas DMAZ is not. In both scenarios, a LOX/quadricyclane RD-180 can increase the payload delivered to LEO by 7–8% over the baseline LOX/RP RD-180. This translates into a payload increase of over 2200 lb to LEO. Quadricyclane is particularly well suited because the baseline tank sizes, sized for a LOX/RP mixture ratio of 2.72, result in a LOX/quadricyclane mixture ratio of 2.24 (due to the fact that quadricyclane is denser than RP). As can be seen in Fig. 18, this mixture ratio is close to the mixture ratio at which I_{sp} is a peak at the RD-180 operating conditions (mixture ratio of ~2.14). This means that either scenario could be employed using quadricyclane as the fuel replacement to achieve substantial performance increases.

Several factors impair the performance of a LOX/DMAZ Atlas V, the most significant is that the DMAZ peak I_{sp} occurs at a much lower

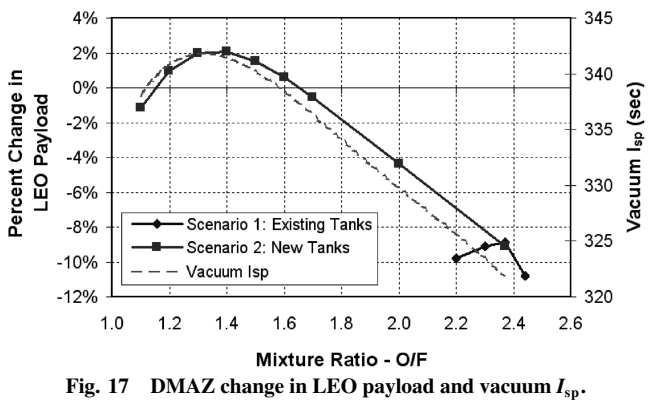

Fig. 17 DMAZ change in LEO payload and vacuum I_{sp}.

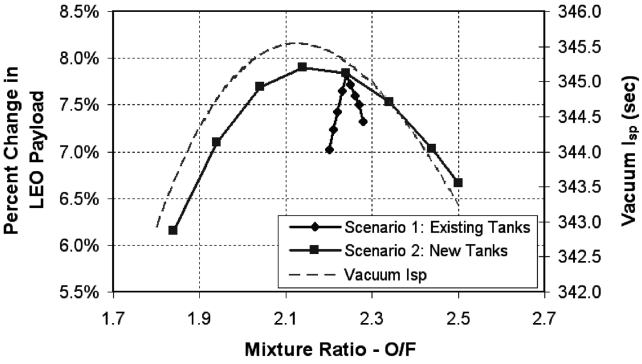

Fig. 18 Quadricyclane change in LEO payload and vacuum I_{sp}.

mixture ratio (~1.3) than either quadricyclane or RP. If the same tanks are used from the baseline RD-180, the mixture ratio with a full propellant load is 2.37. At this mixture ratio, the I_{sp} of a LOX/DMAZ RD-180 is approximately 322 s (down from a peak I_{sp} of 342 s at a mixture ratio of 1.3). This makes DMAZ a poor choice for scenario 1. Even in the second scenario, DMAZ does not provide much of a performance benefit over the baseline LOX/RP Atlas V. This is due to the fact that in order to increase the I_{sp} of a LOX/DMAZ RD-180 engine, the mixture ratio must be lowered. At a mixture ratio range of 1.2–1.6, even though the I_{sp} is 3–4 s higher than the baseline LOX/RP RD-180 I_{sp} (337.8 s), the payload delivered to LEO is only modestly higher (~500 lb). This is because the propellant load (total fuel and oxidizer) is lower. By lowering the mixture ratio, the percentage of propellant that is fuel increases. Because the fuel is less dense than the oxidizer ($\rho_{DMAZ} = 57.6$ lbm/ft^3 and $\rho_{LOX} = 71.2$ lbm/ft^3), by decreasing the mixture ratio while keeping the vehicle dimensions the same (same total propellant volume), the overall propellant load decreases. This decrease in propellant load tends to offset most of the performance benefits gained from the increase in I_{sp}.

IV. Conclusions

A thermophysical property calculation method was developed for use in the conceptual design of rocket engine powerheads employing novel propellants with poorly known properties. This method uses a variety of property prediction techniques, including quantum mechanical energy calculations, molecular dynamic simulations, and group additivity calculations. The method employs a force field model with coefficients that can depend on the propellant. Therefore, the developed method also includes an approach for optimizing these coefficients with a model compound that is somewhat similar to the propellant of interest.

Results have been presented for two high-energy-density matter (HEDM) propellants: DMAZ and quadricyclane. A comparison of these results to experimental data for the thermodynamic properties (density, enthalpy, and entropy) indicates that the method works very well for quadricyclane and reasonably well for DMAZ. Although the optimized force field coefficients improve the DMAZ predictions, there is room for improvement. Some possible reasons for the lack of accuracy in the DMAZ predictions are the choice of model compound, the fit of the density and specific-heat RSEs, and the choice of keeping some possibly influential molecular dynamics intermolecular potential model parameters unchanged. The kinematic viscosity and thermal conductivity results, predicted through group additivity methods, are sufficiently accurate for rocket engine powerhead design codes. Less accuracy is needed for these properties due to their small effect on I_{sp}. For other applications in which the prediction of kinematic viscosity and thermal conductivity require more accuracy, different prediction techniques, such as molecular dynamics, would need to be employed. Additionally, a study of the phase change of compounds would be useful for future work, especially for applications other than conceptual rocket engine powerhead design, such as avoiding pump cavitation when designing turbopumps.

Using the predicted thermophysical properties for quadricyclane and DMAZ, two conceptual vehicle design case studies were performed. The results for the ESAS Lunar Surface Access Module (LSAM) indicate that the use of HEDM propellants may be an attractive option for reducing the LSAM gross weight. The results also indicate that HEDM propellants are superior even to the currently proposed LOX–methane alternative using two different propellant boiloff mitigation scenarios. At the same time, the more detailed analysis made possible by the calculation of thermophysical properties reveals a less favorable case for the HEDM propellants than would have been obtained with the simpler methods normally applied for propellants with minimal property information. The second case study is of the Atlas V 402. The results of this case study indicate that quadricyclane may be an attractive alternative to RP for the Atlas V and has the potential to increase payload delivered to LEO by 7–8%, or over a ton. The results also indicate that DMAZ does not provide the same kind of payload delivery improvements, due to its significantly lower mixture ratio for peak I_{sp}.

The technique presented here allows one to numerically determine the necessary thermophysical properties of potential propellants in order to quantify their impact on conceptual vehicle designs. Armed with this information, one can then make intelligent funding choices based upon the results of these conceptual vehicle design analyses.

Acknowledgments

This work was funded by the University Institute's Institute for Future Space Transport under NASA's Project Constellation. The authors would like to thank the members of the Space Systems Design Lab (SSDL) at the Georgia Institute of Technology.

References

[1] Wucherer, E. J., and Wilson, A., "Chemical, Physical and Hazards Properties of Quadricyclane," U.S. Air Force Research Lab., Rept. PL-TR-97-3053, Edwards AFB, CA, Mar. 1998.

[2] Tishkoff, J. M., and Berman, M. R., "Air Force Basic Research in Propellants and Combustion," AIAA Paper 2002-0901, Jan. 2002.

[3] McQuaid, M. J., "Computational Characterization of 2-Azidocycloalkanamines—Notional Variations on the Hypergol 2-Azido-N,N-Dimethylethanamine (DMAZ)," *Joint Army Navy NASA Air Force 30th Propellant Development and Characterization Subcommittee Meeting*, Chemical Propulsion Information Agency, Columbia, MD, Mar. 2002, pp. 45–57.

[4] McQuaid, M. J., "Structure of Secondary 2-Azidoethanamines: A Hypergolic Fuel vs. a Nonhypergolic Fuel," U.S. Army Research Lab., Rept. ARL-TR-3176, Aberdeen Proving Ground, MD, Apr. 2004.

[5] Bai, S. D., Dumbacher, P., and Cole, J. W., "Development of Advanced Hydrocarbon Fuels at Marshall Space Flight Center," NASA TP-2002-211729, May 2002.

[6] Palaszewski, B., "Solid Hydrogen Experiments for Atomic Propellants: Particle Formation, Imaging, Observations, and Analyses," AIAA Paper 2003-4688, July 2003.

[7] Palaszewski, B., Jurns, J., Breisacher, K., and Kearns, K., "Metallized Gelled Propellants Combustion Experiments in a Pulse Detonation Engine," AIAA Paper 2004-4191, July 2004.

[8] Evans, A. L., Follen, G., Naiman, C., and Lopez, I., "Numerical Propulsion System Simulation's National Cycle Program," AIAA Paper 98-3113, July 1998.

[9] REDTOP-2, Software Package, Ver. 1.85, SpaceWorks Engineering, Inc., Atlanta, 2005.

[10] "System Design Specification for the ROCETS (Rocket Engine Transient Simulation) System," Pratt & Whitney Corp., Rept. FR-20284, West Palm Beach, FL, Aug. 1990.

[11] Rapaport, D. C., *The Art of Molecular Dynamics Simulation*, 2nd ed., Cambridge Univ. Press, Cambridge, England, U.K., 2004, pp. 10–35.

[12] Sun, H., "COMPASS: An Ab Initio Force-Field Optimized for Condensed-Phase Applications—Overview with Details on Alkane and Benzene Compounds," *Journal of Physical Chemistry B*, Vol. 102, No. 38, 1998, pp. 7338–7364. doi:10.1021/jp980939v

[13] Sun, H., and Rigby, D., "Polysiloxanes: Ab Initio Force Field and Structural, Conformational and Thermophysical Properties," *Spectrochimica Acta, Part A (Molecular Spectroscopy)*, Vol. 53, No. 8, 1997, pp. 1301–1323. doi:10.1016/S1386-1425(97)00013-9

[14] Rigby, D., and Sun, H., "Computer Simulations of Poly(ethylene Oxide): Force Field, PVT Diagram and Cyclization Behaviour," *Polymer International*, Vol. 44, No. 3, 1997, pp. 311–330. doi:10.1002/(SICI)1097-0126(199711)44:3<311::AID-PI880>3.0.-CO;2-H

[15] Sun, H., Fried, J. R., and Ren, P., "The COMPASS Force Field: Parameterization and Validation for Phosphazenes," *Computational and Theoretical Polymer Science*, Vol. 8, No. 1, 1998, pp. 229–246. doi:10.1016/S1089-3156(98)00042-7

[16] Kokan, T. S., "Characterizing High-Energy-Density Propellants for Space Propulsion Applications," Ph.D. Dissertation, Georgia Inst. of Technology, Atlanta, 2007.

[17] Lagache, M., Ungerer, P., Bloutin, A., and Fuchs, A. H., "Prediction of Thermodynamic Derivative Properties of Fluids by Monte Carlo Simulation," *Physical Chemistry Chemical Physics*, Vol. 3, No. 19, 2001, pp. 4333–4339. doi:10.1039/b104150a

[18] Cadena, C., Zhao, Q., Snurr, R. Q., and Maginn, E. J., "Molecular Modeling and Experimental Studies of the Thermodynamic and Transport Properties of Pyridinium-Based Ionic Liquids," *Journal of Physical Chemistry B*, Vol. 110, No. 6, 2006, pp. 2821–2832. doi:10.1021/jp056235k

[19] Cadena, C., and Maginn, E. J., "Molecular Simulation Study of Some Thermophysical and Transport Properties of Triazolium-Based Ionic Liquids," *Journal of Physical Chemistry B*, Vol. 110, No. 36, 2006, pp. 18026–18039. doi:10.1021/jp0629036

[20] Schmidt, M. W., Baldridge, K. K., Boatz, J. A., Elbert, S. T., Gordon, M. S., Jensen, J. H., Koseki, S., Matsunaga, N., Nguyen, K. A., Su, S., Windus, T. L., Dupuis, M., and Montgomery, J. A., "General Atomic and Molecular Electronic Structure System," *Journal of Computational Chemistry*, Vol. 14, No. 11, 1993, pp. 1347–1363. doi:10.1002/jcc.540141112

[21] Scott, A. P., and Radom, L., "Harmonic Vibrational Frequencies: An Evaluation of Hartree-Fock, Møller-Plesset, Quadratic Configuration Interaction, Density Functional Theory, and Semiempirical Scale Factors," *Journal of Physical Chemistry*, Vol. 100, No. 41, 1996, pp. 16502–16513. doi:10.1021/jp960976r

[22] Frenkel, D., and Smit, B., *Understanding Molecular Simulation, from Algorithms to Applications*, Academic Press, San Diego, CA, 1996, pp. 18–21.

[23] van Wylen, G., Sonntag, R., and Borgnakke, C., *Fundamentals of Classical Thermodynamics*, Wiley, New York, 1994, pp. 150–154.

[24] Joback, K. G., *Cranium: Component Software for Physical Property Estimation*, Molecular Knowledge Systems, Inc., Bedford, NH, 1998.

[25] Benson, S. W., *Thermochemical Kinetics: Methods for the Estimation of Thermochemical Data and Rate Parameters*, 2nd ed., Wiley, New York, 1976, pp. 132–138.

[26] Benson, S. W., and Buss, J. H., "Additivity Rules for the Estimation of Molecular Properties, Thermodynamic Properties," *Journal of Chemical Physics*, Vol. 29, No. 3, 1958, pp. 546–572. doi:10.1063/1.1744539

[27] Chung, T.-H., Ajlan, M., Lee, L. L., and Starling, K. E., "Generalized Multiparameter Correlation for Nonpolar and Polar Fluid Transport Properties," *Industrial and Engineering Chemistry Research*, Vol. 27, No. 4, 1988, pp. 671–679. doi:10.1021/ie00076a024

[28] Bleazard, J. G., "The Thermal Conductivity of Aqueous Electrolyte Solutions and Polar Liquids," Ph.D. Dissertation, Georgia Inst. of Technology, Atlanta, 1995.

[29] Osmont, A., and Catoire, L., "Evaluating Missile Fuels," *Propellants, Explosives, Pyrotechnics*, Vol. 31, No. 5, 2006, pp. 343–354. doi:10.1002/prep.200600043

[30] Stevenson, W. H., "Synthesis and Characterization of Hypergolic Amino Azides," *Joint Army/Navy/NASA/Air Force 30th Propellant Development and Characterization Subcommittee Meeting*, Chemical Propulsion Information Agency, Columbia, MD, Mar. 2002, pp. 95–102.

[31] "NASA Exploration Systems Architecture Study Final Report," NASA TM-2005-214062, Nov. 2005.

[32] Plachta, D. W., "Zero Boiloff Storage of Cryogenic Propellants Achieved at Lewis' Supplemental Multilayer Insulation Research Facility" [online article], http://www.grc.nasa.gov/WWW/RT1998/5000/5870plachta.html [retrieved Jan. 2007]..

[33] Humble, R. W., Henry, G. N., and Larson, W. J., *Space Propulsion Analysis and Design*, McGraw–Hill, New York, 1995, pp. 270–280.

[34] Wertz, J. R., and Larson, W. J., *Space Mission Analysis and Design*, Microcosm Press, El Segundo, CA, 1999, pp. 430–450.
[35] Brauer, G. L., Cornick, D. E., Habeger, A. R., Petersen, F. M., and Stevenson, R., "Program to Optimize Simulated Trajectories (POST)," Martin Marietta Corp., Denver, CO, 1975.
[36] Rohrschneider, R. R., "Development of a Mass Estimating Relationship Database for Launch Vehicle Conceptual Design," M.S., Thesis, Georgia Inst. of Technology, Atlanta, GA, 2002.
[37] "RL-10," Pratt & Whitney Corp., Rept. TS 9.01, West Palm Beach, FL, 1999.
[38] Gordon, S., and McBride, B. J., "Computer Program for Calculation of Complex Chemical Equilibrium Compositions and Applications 1: Analysis," NASA RP-1311, 1994.
[39] REDTOP, Software Package, Ver. 1.2, SpaceWorks Engineering, Inc., Atlanta, 2004.
[40] Way, D., and Olds, J., "SCORES: Web-Based Rocket Propulsion Analysis for Space Transportation System Design," AIAA Paper 1999-2353, June 1999.
[41] Isakowitz, S. J., Hopkins, J. P., Jr., and Hopkins, J. B., *International Reference Guide to Space Launch Systems*, AIAA, Reston, VA, 1999, pp. 55–74.
[42] Guynn, M. D., "Aerodynamic Preliminary Analysis System, Beginner's Guide," NASA Langley Research Center, Hampton, VA, 1989.